



## Article

# Sidelobes Suppression for Time Domain Anti-Jamming of Satellite Navigation Receivers

Wenxiang Liu <sup>1</sup>, Zukun Lu <sup>1,\*</sup> , Zhiying Wang <sup>1,2</sup>, Xianghao Li <sup>1</sup>, Zongnan Li <sup>1</sup>, Wei Xiao <sup>1</sup>, Xiaozhou Ye <sup>1</sup>, Zhi Wang <sup>3</sup>, Jie Song <sup>1</sup>, Jia Qiao <sup>1</sup> and Baiyu Li <sup>1</sup>

<sup>1</sup> College of Electronic Science and Technology, National University of Defense Technology, Changsha 410073, China

<sup>2</sup> Beijing Satellite Navigation Center, Beijing 100080, China

<sup>3</sup> Transcom (Shanghai) Technology Co., Ltd., Shanghai 201601, China

\* Correspondence: luzukun@nudt.edu.cn; Tel.: +86-155-7499-3958

**Abstract:** The global satellite navigation system represented by global position systems (GPS) has been widely used in civil and military fields, and has become an important cornerstone of space-time information services. However, the frequency band of satellite navigation signals is open, and the frequency points overlap with some radars and communication systems, which brings challenges to the application of satellite navigation. Time-domain adaptive filtering technology is a typical anti-jamming method which can suppress the narrow-band interference faced by satellite navigation. However, in the process of suppressing narrow-band interference, the navigation signal will be distorted, which is mainly reflected in the distortion of the spectrum of the navigation signal, which will lead to the enhancement of the side lobes in the correlation function. In this paper, we focus on time-domain adaptive anti-jamming, study the mechanism of correlation function sidelobes lift caused by narrow-band interference suppression, and propose a correlation function sidelobes suppression method based on time-domain adaptive anti-jamming, which can be realized without losing anti-jamming performance. The simulation experiment verifies the validity of the mechanism analysis of the sidelobes lift of the correlation function and the effectiveness of the proposed method. The analysis results and the proposed method are of great significance, which is reflected in the improvement of the anti-jamming performance and acquisition performance of satellite navigation receivers.

**Keywords:** GPS; time-domain adaptive anti-jamming; sidelobes suppression; signal reconstruction; correlation function



**Citation:** Liu, W.; Lu, Z.; Wang, Z.; Li, X.; Li, Z.; Xiao, W.; Ye, X.; Wang, Z.; Song, J.; Qiao, J.; et al. Sidelobes Suppression for Time Domain Anti-Jamming of Satellite Navigation Receivers. *Remote Sens.* **2022**, *14*, 5609. <https://doi.org/10.3390/rs14215609>

Academic Editor:  
Andrzej Stateczny

Received: 22 September 2022

Accepted: 3 November 2022

Published: 7 November 2022

**Publisher's Note:** MDPI stays neutral with regard to jurisdictional claims in published maps and institutional affiliations.



**Copyright:** © 2022 by the authors. Licensee MDPI, Basel, Switzerland. This article is an open access article distributed under the terms and conditions of the Creative Commons Attribution (CC BY) license (<https://creativecommons.org/licenses/by/4.0/>).

## 1. Introduction

The Global Navigation Satellite System (GNSS) is satellite-based all-weather navigation, positioning, and timing system [1,2]. At present, the satellite navigation systems in the world mainly include the GPS (Global Positioning System) of the United States, the Beidou satellite navigation system of China, the GLONASS (Global Navigation Satellite System) of Russia, and the Galileo system of Europe [3–6]. With the deterioration of the electromagnetic environment and the escalation of the intensity and complexity of interference, the concepts of electronic warfare and navigation warfare have received much attention with regard to modern combat systems, and higher standards are put forward for the anti-jamming ability of the navigation receiver [7–9]. Thus, the navigation equipment must have a strong anti-jamming ability.

Diverse space electromagnetic environments and man-made electromagnetic interference are the main sources of interference faced by satellite navigation receivers. Man-made electromagnetic interference includes intentional interference and unintentional interference [10,11]. The L band in unintentional interference coincides with the terrestrial radar band, and the navigation system is susceptible to jamming [12]. The most typical jamming scenarios in intentional jamming are narrowband jamming and broadband jamming, both

of which will affect the performance of the navigation system and even lead to system paralysis in severe cases [13–16]. From the perspective of the entire navigation system, since the optimization of the signal system and the improvement of the transmission power have been determined in the early stage of the construction of the navigation system, the task of improving the anti-jamming performance at this stage falls on the satellite navigation receiver of the receiving terminal [17–20].

Common anti-jamming technologies can be divided into time-frequency domain anti-jamming technology based on the single antenna, space-domain anti-jamming technology based on the antenna array, and anti-jamming technology combining space-time and space-frequency [21–23]. Antenna array anti-jamming technology uses multiple antenna array elements and uses vector weighting to cancel interference according to the different signal direction angles and interference direction angles [24,25]. Different from single-antenna anti-jamming technology, it can suppress broadband interference [26]. Compared with antenna array anti-jamming technology, the single antenna has irreplaceable advantages in some application backgrounds. It is mainly reflected in the small size of the single antenna, which can be customized according to the shape of the installation platform [27]. It has fewer receiver channels, a simpler hardware structure, low power consumption, and high-cost performance. The ranging error caused by mutual coupling and channel mismatch between array elements does not require complex channel correction. Therefore, the single antenna is widely used in most high-precision receivers.

Anti-jamming in the time-frequency domain will cause the sidelobes of the correlation function to rise [28]. In 2016, Fan Guangteng analyzed the principle of sidelobes lift of the correlation function from the frequency domain [29]. It equals the anti-jamming filter as an ideal band-stop filter and decomposes it into the difference between the all-pass filter and the band-pass filter. From the perspective of the frequency domain, the splitting of the signal spectrum after anti-jamming will inevitably lead to the rise of the sidelobes of the correlation peak. The rise of the sidelobes is directly related to the interference characteristics, but the interference characteristics are uncertain. However, the effects of frequency domain and time domain anti-jamming are both analyzed in the frequency domain, and the time-domain anti-jamming is the analysis of the time domain filter equivalent to the frequency domain, and the effect of the anti-jamming algorithm on the correlation peak is the same as that of the interference frequency and bandwidth. The sidelobes lift mechanism caused by the traditional time-domain anti-jamming algorithm still needs further theoretical analysis and elaboration.

The rise of the correlation peak sidelobes will affect the capture of the navigation signal, so the correlation peak sidelobes suppression under the anti-jamming condition in the time-frequency domain has become a research direction [30–32]. Scholars such as Blinchikoff and Park proposed two types of sidelobes suppression filters, discrete and combined [33]. The difference is that the former is a cascade of anti-jamming filters and sidelobes suppression filters, while the latter is designed as a filter that takes into account both anti-jamming and sidelobes suppression needs. Based on the above technologies, Dr. Li Zhengrong proposed a sidelobes suppression filter method based on constant interference loss and applied this method to the sidelobes suppression of anti-jamming receivers [34]. However, in the above-mentioned paper, the sidelobes suppression filters of various structures are designed to suppress the sidelobes under the premise of sacrificing the anti-jamming performance, and the suppression level is limited.

In this paper, under the background of time-domain adaptive anti-jamming, the reasons for the sidelobe's rise of navigation signal caused by time-domain adaptive anti-jamming are deeply analyzed, and the method of sidelobes suppression is proposed. The structure of this paper is as follows. Section 2 introduces the mathematical models studied in this paper, including the signal model and the time-domain adaptive anti-jamming model. The third section analyzes the mechanism of the sidelobes lift of the navigation signal caused by anti-jamming. Section 4 proposes a method for suppressing sidelobes lift

caused by anti-jamming. Section 5 verifies the analysis results and the sidelobes suppression method in this paper by simulation. Finally, the conclusion of this paper is given.

## 2. Mathematical Model

### 2.1. Signal Model

Time-domain adaptive anti-jamming technology uses the strong correlation characteristics of narrowband interference. The navigation signal is a spread spectrum signal and belongs to a wideband signal, and the weak correlation is not easily estimated. The narrowband interference is estimated from the received signal and then canceled from the received signal in a canceling manner. The discrete expression for the received signal is:

$$x(k) = S(k) + I(k) + N(k) \quad (1)$$

where  $k = \dots, -2, -1, 0, 1, 2, \dots$ .  $S(k)$ ,  $I(k)$  and  $N(k)$  represent the navigation signal, interference signal and noise signal, respectively.

The expression for the navigation signal is:

$$S(k) = AD(k)c(k) \quad (2)$$

Among them,  $A$  is the amplitude, and  $D(k)$  is the modulated navigation signal. The subsequent analysis in this paper is all carried out within one bit of relevant accumulation time, so it can be assumed that  $D(k) = 1$ ,  $c(k)$  is a pseudo-random noise code.

$N(k)$  is white Gaussian noise and its complex form is expressed as:

$$N(k) = N_i(k) + i \cdot N_q(k) \quad (3)$$

where,  $N_i(k)$  and  $N_q(k)$  are Gaussian white noise with a bilateral power spectral density equal to  $N_0$ ,  $N_i(k)$  and  $N_q(k)$  are independent of each other.

Under ideal conditions, the pseudo-code autocorrelation function  $R_0(\tau)$  of BPSK (Binary Phase Shift Keying) signal is a triangular wave  $\Lambda(\tau/T_c)$ , and its expression is as follows [35]:

$$R_0(\tau) = \begin{cases} R_{T_c}(\tau), & |\tau| \leq T_l \\ 0, & |\tau| > T \end{cases} \quad (4)$$

where,  $R_{T_c}(\tau) = 1 - \frac{|\tau|}{T_c}$ .

Taking the Beidou B3I signal as an example, the spectral relationship between noise, signal and interference is shown in Figure 1. Figure 1a shows the spectrum of noise, signal, and interference, and Figure 1b shows the synthesized spectrum.

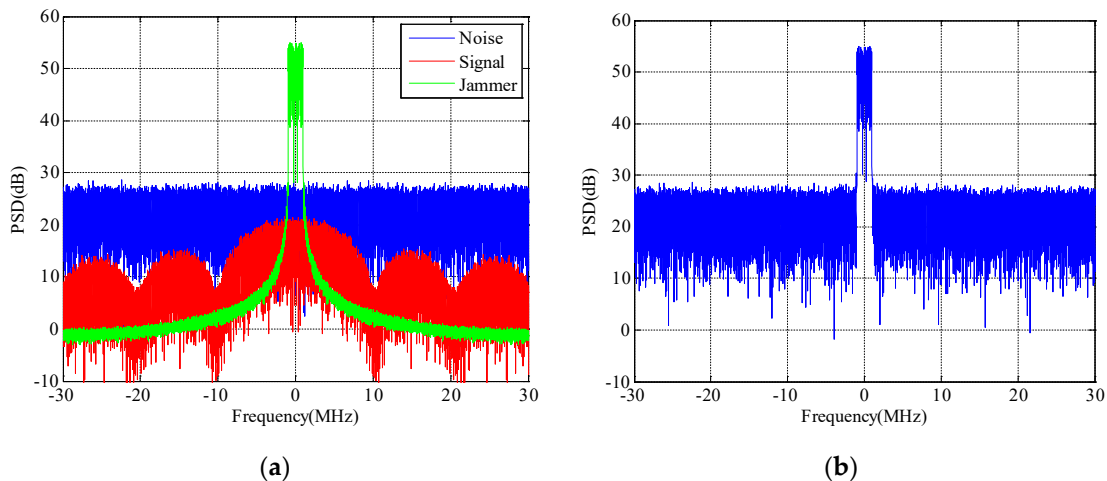


**Figure 1.** Spectrum comparison of interference, signal and noise. (a) Independent shown, (b) Synthetic shown.

The code rate of the Beidou B3I signal is 10.23 MHz, and its signal bandwidth is 20.46 MHz. The autocorrelation characteristics of the navigation signal are shown in Figure 2.

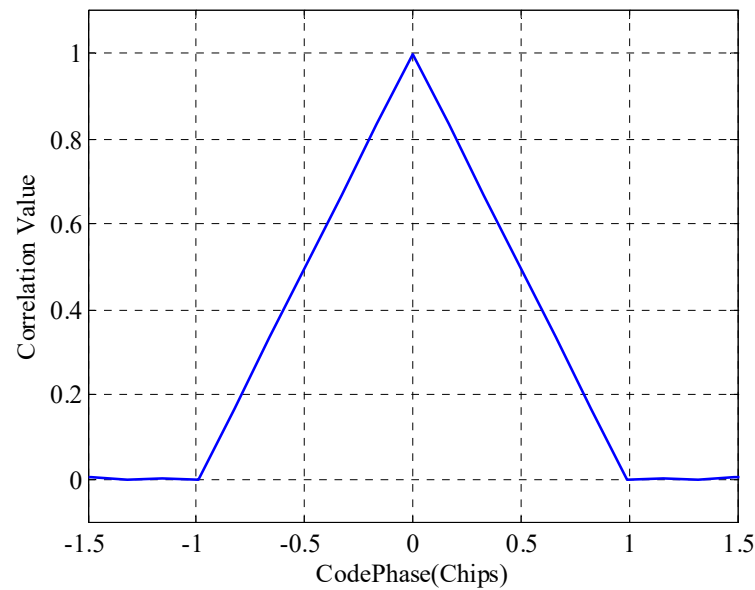


**Figure 2.** Autocorrelation characteristics of navigation signals.

### 2.2. Time-Domain Anti-Jamming Model

The structure of the single-antenna-based time-domain adaptive anti-jamming filter is shown in Figure 3.

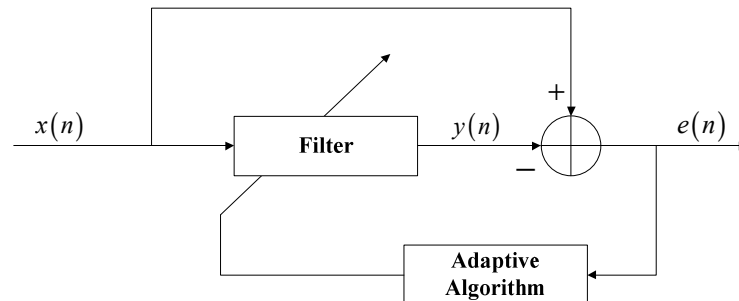


**Figure 3.** Time-domain anti-jamming filter structure.

Common adaptive algorithms for time-domain anti-jamming include the Least Mean Square (LMS) algorithm based on the Minimum Mean Square Error (MMSE) criterion and the Least Squares (LS) algorithm based on the Recursive Least Squares (RLS) algorithm. Among them, the LMS algorithm proposed by Widrow and Hoff in 1957 has the advantages of simple principle and no need for complex matrix inversion and is widely used [36]. The LMS algorithm is a classical anti-jamming processing algorithm and also a commonly used one. This algorithm is widely used in satellite navigation receivers. This article only analyzes the LMS algorithm.

Let the output signal be  $y(n)$ , the output data of the filter be  $y(k)$ , then we can get:

$$y(k) = \mathbf{w}^H(k)\mathbf{x}(k) \quad (5)$$

Among them,  $\mathbf{w}(k)$  represents the filter weight vector at time  $k$ .  $\mathbf{x}(k)$  represents the sampled data vector input by the filter.

Let  $d(k)$  be the desired signal of the filter, then the error of the filter can be expressed as:

$$e(k) = d(k) - y(k) = d(k) - \mathbf{w}^H(k)\mathbf{x}(k) \quad (6)$$

The iterative formula for the weight coefficient of the LMS algorithm is as follows:

$$\mathbf{w}(k + 1) = \mathbf{w}(k) + \mu \mathbf{x}(k)\mathbf{e}^*(k) \tag{7}$$

Among them,  $\mu$  is the step factor, and its value must satisfy:

$$0 < \mu < 2/\lambda_{\max} \tag{8}$$

where,  $\lambda_{\max}$  is the maximum eigenvalue of the correlation matrix between the navigation signal and the local pseudocode, and the algorithm can only be converged when the step factor satisfies Equation (8).

The filter structure used in this paper is a commonly used odd-order bilateral tap transversal filter, that is, a filter with an interpolation structure. Constraining the full coefficient of the middle tap to always be 1 is to ensure that the weight vector does not converge to all zeros. The filter architecture is shown in Figure 4, where  $[\ ]^*$  represents the conjugation.

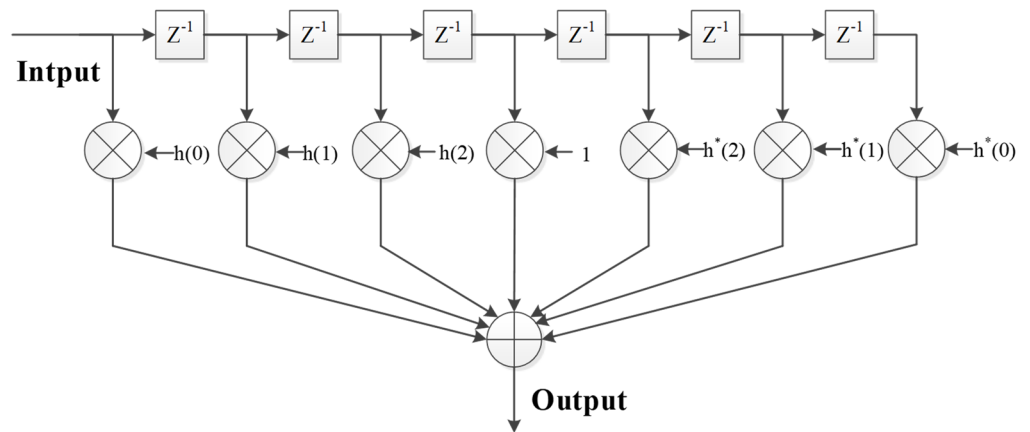


Figure 4. Architecture of the time-domain anti-jamming filter.

In the interference scenario shown in Figure 1, the time-domain adaptive anti-jamming technology is used, and the spectrum after anti-jamming is shown in Figure 5.

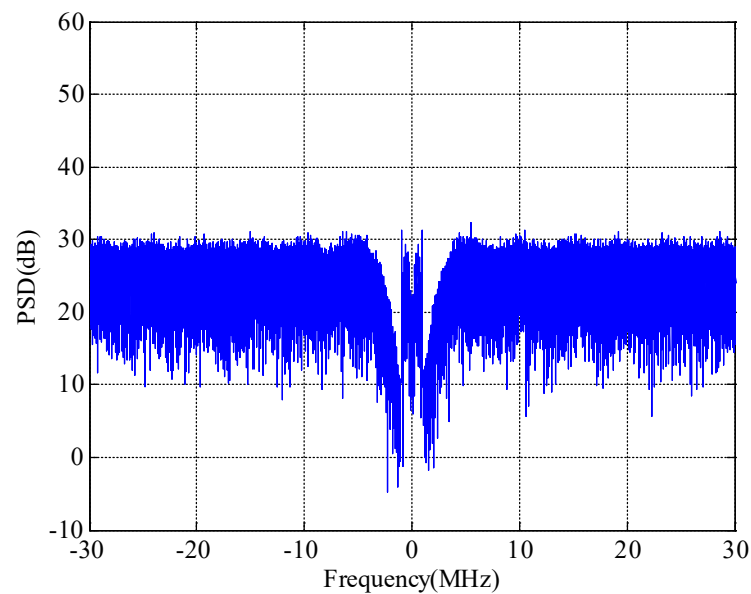


Figure 5. Spectrum after anti-jamming in the frequency domain.

### 3. Mechanism Analysis of Sidelobes Lift

From the perspective of the frequency domain, much literature has analyzed the reasons for the raised sidelobes of the correlation peak. The classic model used is usually equivalent to an ideal band-stop filter, which is obtained by subtracting the band-pass filter from the all-pass filter, as shown in Figure 6.

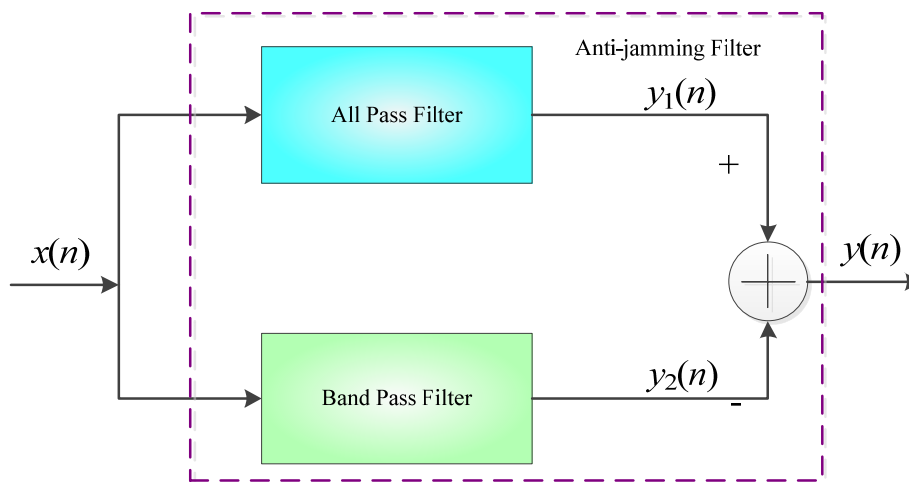


Figure 6. Schematic diagram of anti-jamming filter decomposition.

For an all-pass filter, its discrete impulse response is  $\delta(n)$ , and the time-domain discrete impulse response expression of an ideal band-pass filter is  $\frac{\sin \omega_c n}{\pi n} e^{-j\omega_0 n}$ , where  $\omega_c$  is the single-sideband bandwidth and  $\omega_0$  is the interference center frequency.

The discrete impulse response of the band pass filter is subtracted from the discrete impulse response of the ideal all pass filter, and the discrete impulse response of the anti-jamming filter is obtained as follows [37]:

$$h_{anti-jam}(n) = \begin{cases} 1 - \frac{\omega_c}{\pi}, & n = 0 \\ \frac{\sin \omega_c n}{\pi n} e^{-j\omega_0 n}, & n \neq 0 \end{cases} \tag{9}$$

However, the effects of frequency-domain and time-domain anti-jamming on sidelobes are both analyzed in the frequency domain, and the time-domain anti-jamming is the analysis of the time-domain filter equivalent to the frequency domain. Therefore, this paper will further analyze the mechanism of the correlation peak sidelobes lift caused by the traditional anti-jamming algorithm in the time domain. From the perspective of the correlation domain, the correlation function is expressed as follows:

$$\begin{aligned} R(\tau) &= \sum_{k=-M}^M w_k R_{xs}(\tau + k \cdot \tau_0) \\ &= w_{-M} R_{xs}(\tau - M \cdot \tau_0) + \dots + \\ &\quad w_{-1} R_{xs}(\tau - \tau_0) + w_0 R_{xs}(\tau) + \\ &\quad w_1 R_{xs}(\tau + \tau_0) + \dots + w_M R_{xs}(\tau + M \cdot \tau_0) \end{aligned} \tag{10}$$

As can be seen from the above formula, under the time-domain anti-jamming algorithm, the formation of sidelobes of the correlation function is also formed by the superposition of delayed correlation functions at different times. The sidelobes peak value of the correlation peak is related to the anti-jamming filter coefficient. The delay correlation functions at different times formed under the real weights are shown in Figure 7.

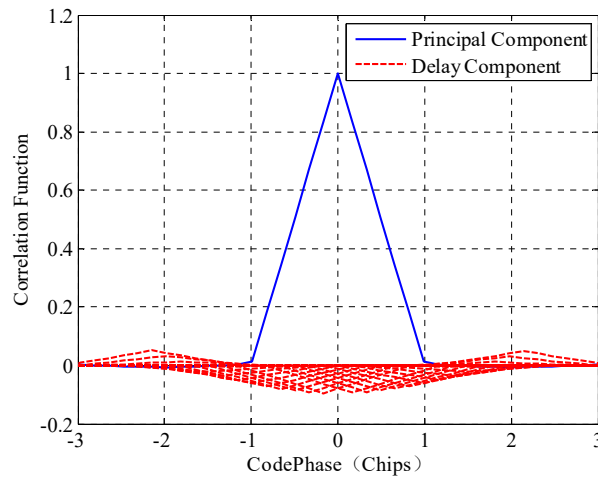


**Figure 7.** Correlation peak sidelobes formation diagram in traditional LMS algorithm.

The lifting mechanism of time-domain anti-jamming on correlation peak sidelobes is attributed to the superposition of signals at different time delays. Due to the change of the anti-jamming filter coefficient under different interference frequencies and bandwidths, the correlation peak sidelobes will have different effects under these conditions. Under the condition of anti-jamming, the relationship between the power spectrum of the navigation signal and the correlation function is as follows [38]:

$$R(\tau) = \int_{-\infty}^{+\infty} H(f)S(f)e^{j2\pi f\tau}df \tag{11}$$

Among them,  $H(f)$  is the frequency domain expression of the anti-jamming filter, and  $S(f)$  is the power spectral density function of the signal.

From the above formula, it can be concluded that under the conditions of different interference bandwidths and interference frequencies, the correlation function will be affected. The influence of anti-jamming on the correlation function under different conditions is shown in Figures 8 and 9.

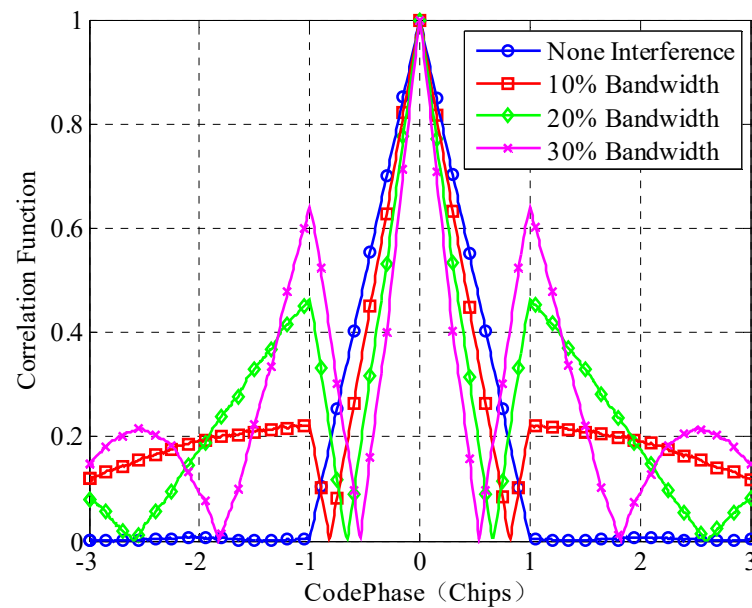


**Figure 8.** Influence of correlation function under different interference bandwidths.

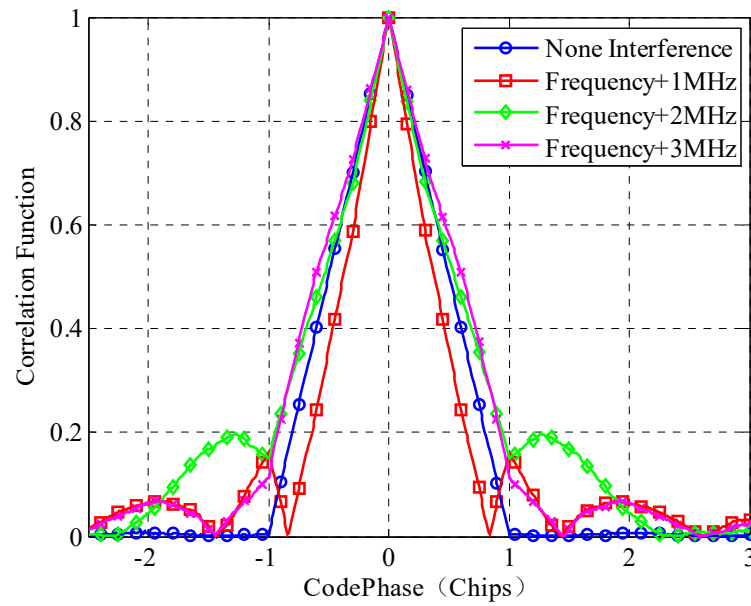


Figure 9. Influence of correlation function at different interference frequencies.

#### 4. Sidelobes Suppression Technology

##### 4.1. Correlation Peak Model

From the perspective of the correlation domain, the core idea of the algorithm is to use the coefficient  $w_i$  and estimated amplitude  $A_R$  of the anti-jamming filter to reconstruct the delay correlation function with the local signal. Subtract the reconstructed local signal components  $\hat{s}(n \pm i)$  at different delay times from the signal  $y(n)$  after the anti-jamming module to obtain a new output signal  $y'(n)$ , and then perform secondary acquisition of the signal. When  $y'(n)$  is correlated with the local pseudocode signal, the delay component of the correlation function superimposed by the adaptive anti-jamming algorithm is canceled in order to achieve the purpose of sidelobes suppression. The correlation function  $R_{SLS}(\tau)$  after bypass inhibition can be expressed and shown as:

$$\begin{aligned}
 R_{SLS}(\tau) &= \sum_{n=-\infty}^{\infty} \{ [y(n) - \hat{s}(n \pm i)] s^*(n - \tau - \Delta\tau) \} \\
 &= \sum_{n=-\infty}^{\infty} \{ [y(n) - A_R \sum_{\substack{k=-M \\ k \neq 0}}^M w_k s(n - k - \Delta\tau)] s^*(n - \tau - \Delta\tau) \} \\
 &= \sum_{n=-\infty}^{\infty} y(n) s^*(n - \tau - \Delta\tau) - \sum_{n=-\infty}^{\infty} [A_R \sum_{\substack{k=-M \\ k \neq 0}}^M w_k s(n - k - \Delta\tau)] s^*(n - \tau - \Delta\tau) \quad (12) \\
 &= R(\tau + \Delta\tau) - A_R \sum_{\substack{k=-N \\ k \neq 0}}^N w_k R_0(\tau + k\tau_0)
 \end{aligned}$$

where,  $N$  is the number of single-side reconstructed signal components, in the bilateral tap transversal filter, the total number of reconstructions is  $2N$ , and the value range of is  $N \leq M$ .  $R_0(\tau)$  is the ideal pseudocode autocorrelation function  $\Lambda(\tau/T_c)$ .  $A_R$  can be estimated as the peak value  $R(0)$  of the correlation function between the output signal after anti-jamming and the local signal each time, and  $\Delta\tau$  is the code phase delay deviation between the received signal and the local replica signal during acquisition.

The  $y'(n)$  correlation with the local signal is equivalent to the correlation function of the anti-jamming output signal and the local signal minus the delay components of the correlation function at different times in the correlation domain. Its equivalent effect diagram is shown in Figure 10. Since the sidelobes suppression algorithm processes the correlation function in the correlation domain in the acquisition stage, it will not affect the anti-jamming performance.

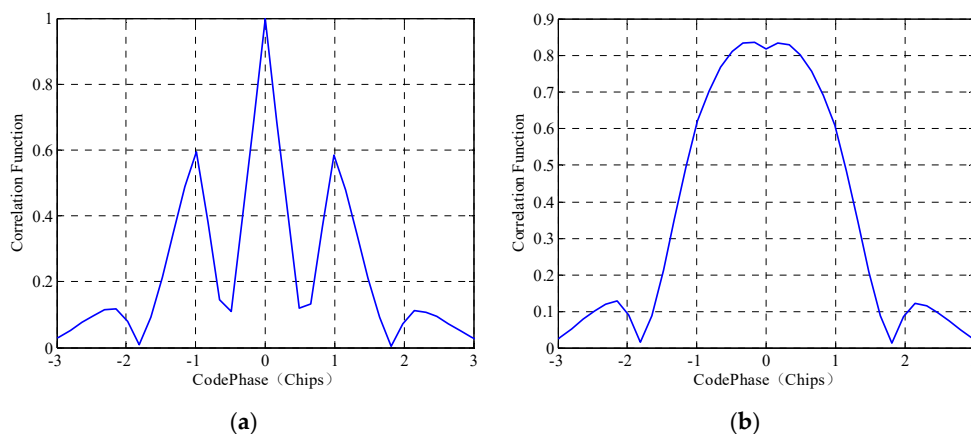


**Figure 10.** Equivalent effect diagram of sidelobes suppression. (a) Correlation function after anti-jamming, (b) Delay component of correlation function.

4.2. Sidelobes Suppression

The block diagram of sidelobes suppression is shown in Figure 11.

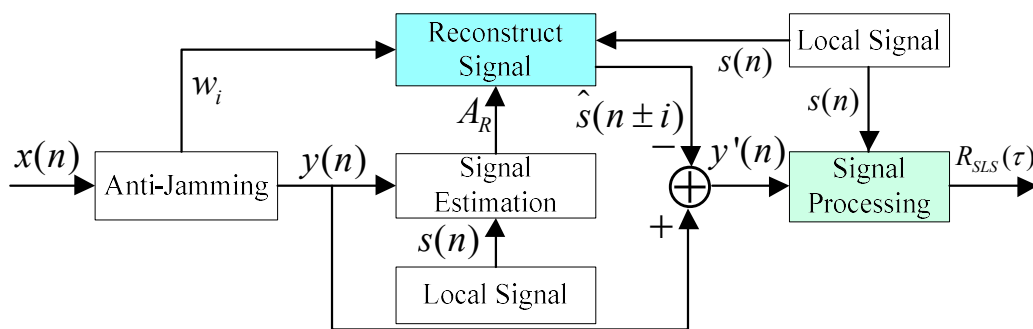


**Figure 11.** Block diagram of sidelobes suppression.

In Figure 11, according to Equation (12), the sidelobe is caused by the superposition of multiple correlation peaks, which are caused by the anti-jamming filter. Therefore, the sidelobe can be suppressed through the anti-jamming filter and the local signal. To put it simply, the signal components caused by anti-jamming are reconstructed and deducted in signal processing. The reconstructed signal component includes two factors, one is the weight coefficient of the anti-jamming filter, and the other is the amplitude estimation of the signal.

The estimation of the signal amplitude adopts the result of the acquisition stage, and the signal search and acquisition algorithm adopts the parallel code phase search [39,40], as shown in Figure 12. After the carrier signal is mixed, the Fourier transform is directly performed on the mixing result, and then the transform result is multiplied by the conjugate of the C/A code Fourier transform, and the correlation value in the time domain is obtained by using the inverse Fourier transform. When the correlation value exceeds the preset threshold, it is determined that the acquisition is successful, and the correlation value at this time is the estimated amplitude of the signal.

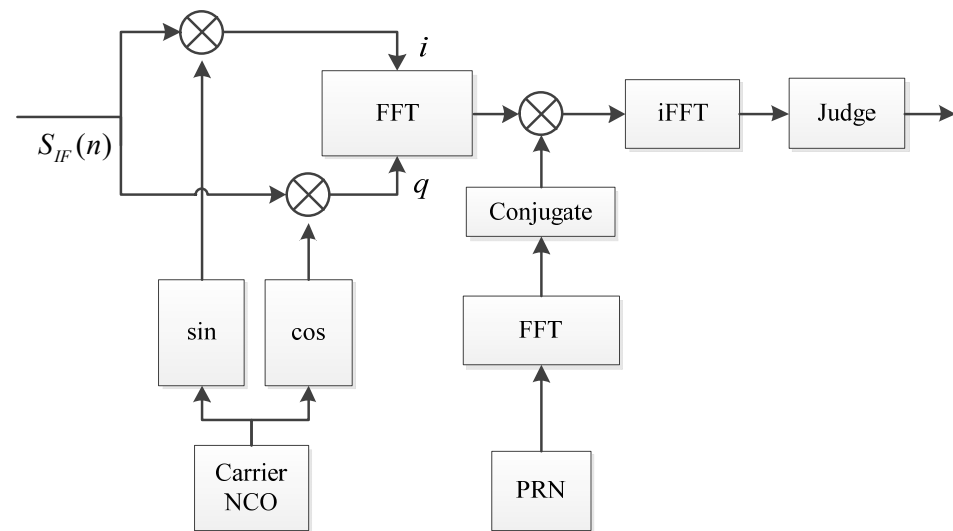


**Figure 12.** Schematic diagram of the acquisition process of the parallel code phase algorithm.

As shown in Figure 12, the parallel code phase search acquisition algorithm mainly includes the following steps:

- (1) According to the frequency grid division, multiply the anti-jamming digital intermediate frequency signal by the frequency carrier to complete the mixing.
- (2) Perform N-point Fast Fourier Transform (FFT) on the mixed signal (if the number of points is less than N, it needs to be filled with zeros).
- (3) Perform complex conjugate processing on the FFT transformation result of the locally copied pseudocode, and multiply it with the FFT transformation of the mixing output signal.
- (4) Perform Inverse Fast Fourier Transform (IFFT) on the result of step (3) to obtain the cross-correlation result between the received signal and the local spread spectrum signal.
- (5) Perform absolute value judgment on the result of (4). If it exceeds the threshold, it is considered that the acquisition is successful, and the code phase and frequency estimation value are outputted, otherwise steps (3), (4), and (5) are repeated, and the new frequency is searched until the search is complete.

## 5. Simulation Experiment

### 5.1. Effect of Reconstruction Number on Sidelobes Suppression

As shown in Equation (10), the rise of the side lobes of the correlation function is due to the superposition of the delay components of the correlation function at different times during the iterative process of the time-domain anti-jamming algorithm. Therefore, the degree of sidelobes suppression is closely related to the number of signal reconstructions.

Under the simulation condition that the interference bandwidth is 20% of the signal bandwidth and the frequency is located at the center frequency of the navigation signal, the sidelobes suppression process of the correlation function is shown in Figure 13. Correlation functions after sidelobe suppression are compared. It can be seen that with the increase in the reconstruction number of delayed signal components, the first side lobe and the second side lobe are gradually suppressed, the bandwidth of the main lobe is broadened, and the energy is enhanced. When the code phase deviation between the received signal and the local signal is zero when the reconstruction number of the signal component is increased to the same order as the anti-jamming filter, the sidelobes can be suppressed to the noise level, and the correlation function can be restored to the level without interference.

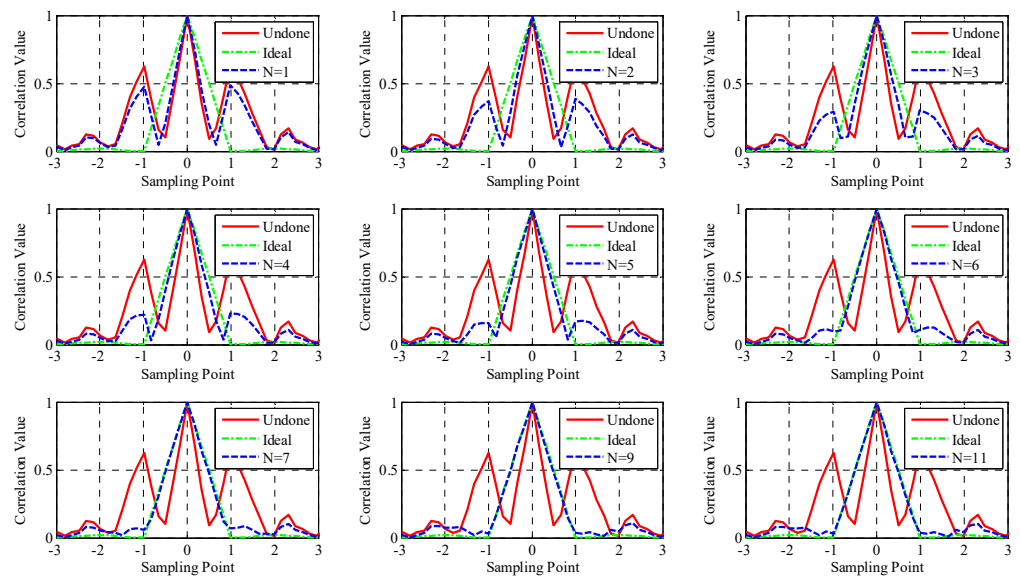


**Figure 13.** Comparison of sidelobes suppression effects under different reconstructed numbers.

5.2. Effect of Interference Bandwidth on Sidelobes Suppression

When the number of unilateral signal reconstructions is 10, sidelobes suppression is performed for the interference of different bandwidths, and the same navigation signal and noise signal are used for it, and the delay error between the received signal and the local pseudocode signal is not considered. Figures 14 and 15 show the received signal spectrum before and after anti-jamming, respectively. The results before and after the suppression of different interference bandwidths are shown in Figure 16. It can be seen from the figure that the anti-jamming processing achieves effective interference suppression, and the correlation function sidelobes under different bandwidth interferences can be effectively suppressed.

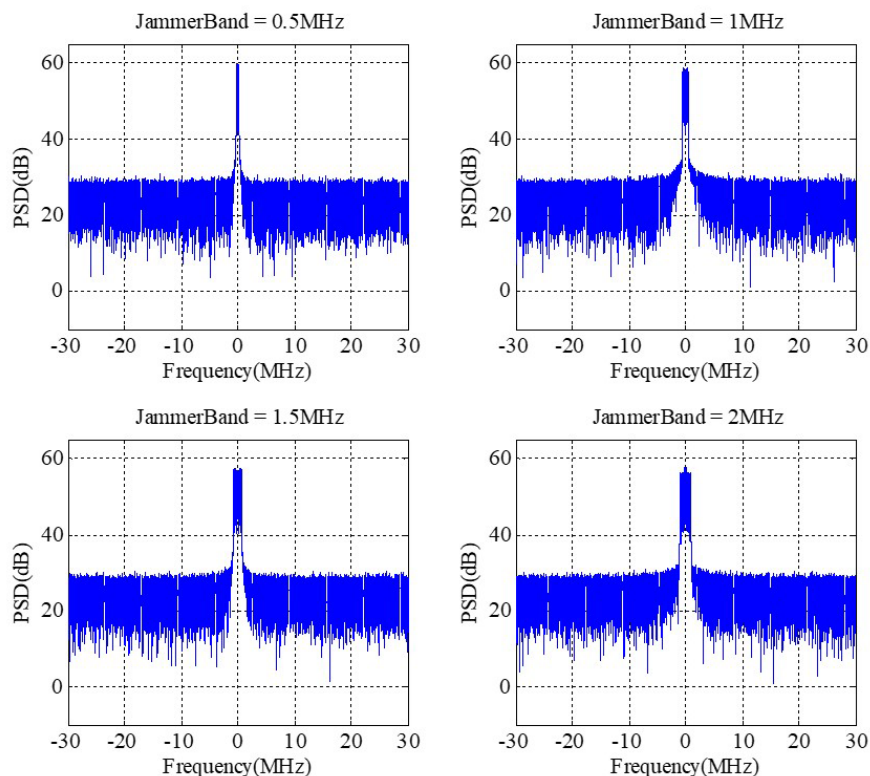


**Figure 14.** Spectral characteristics before anti-jamming in difference interference bandwidths.

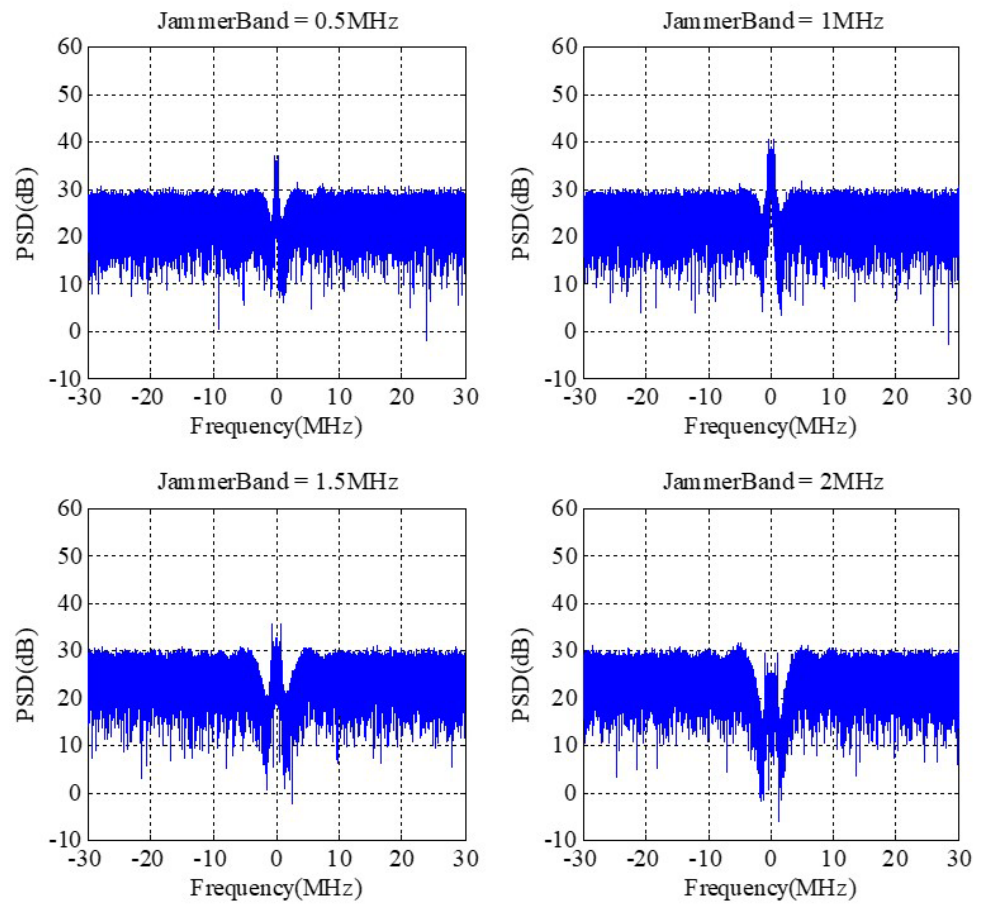


Figure 15. Spectral characteristics after anti-jamming in difference interference bandwidths.

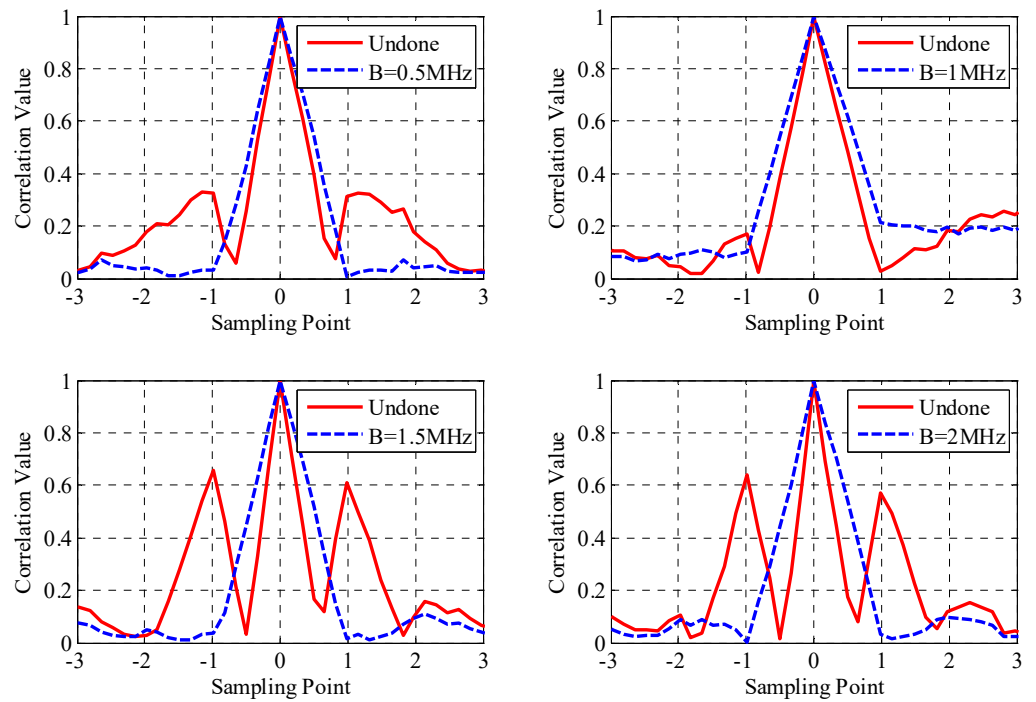


Figure 16. Sidelobes suppression results under different interference bandwidths.

### 5.3. Effect of Amplitude Estimation Accuracy

As shown in Equation (12), the accuracy of the estimated amplitude also affects the sidelobes suppression results. In this simulation, under the interference of 20% of the signal bandwidth, the interference frequency is aligned with the center frequency of the signal, and the sidelobes are suppressed under the unbiased code phase. The suppression results are shown in Figure 17. As can be seen from Figure 17, under the sidelobes suppression algorithm proposed in this paper, as the accuracy of the estimated amplitude decreases, the sidelobes suppression level also decreases.

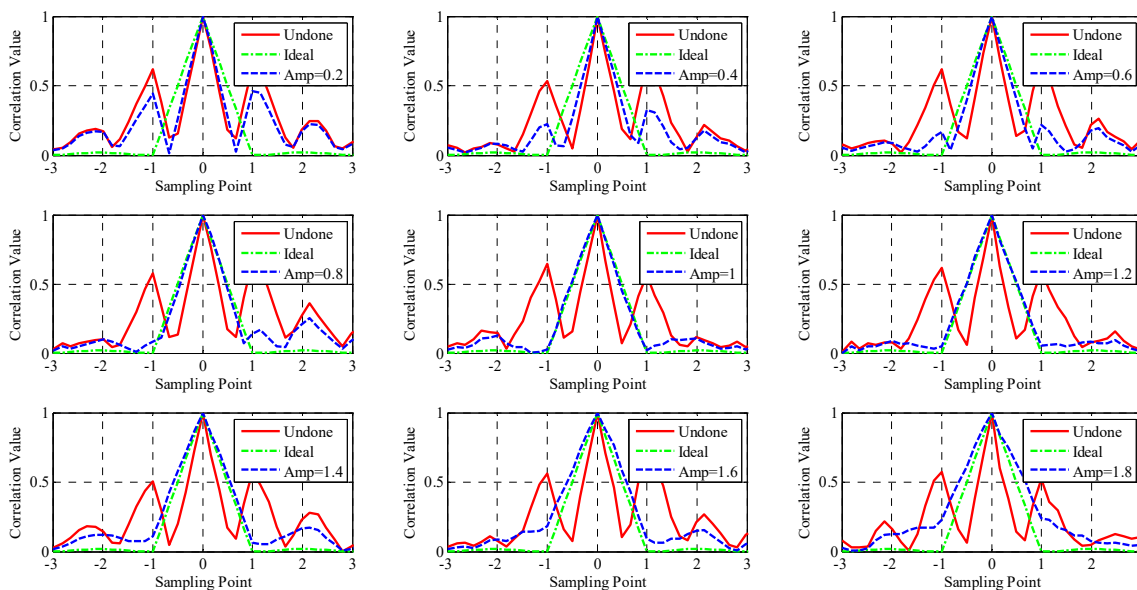


Figure 17. Sidelobes suppression results under different amplitude estimation accuracy.

## 6. Discussion

In the case of narrow-band interference, time-domain adaptive anti-jamming can effectively suppress narrow-band interference, but spectrum splitting occurs in the process of interference suppression, which leads to the rise of the sidelobes of the correlation function. According to the sidelobes suppression method proposed in this paper, the problem of sidelobes boosting can be solved by the method of signal reconstruction. The signal reconstruction order is closely related to the order of the anti-jamming filter. According to the simulation experiment, the reconstruction order does not need to be accurate as long as it meets a certain range. In the simulation scenario of this paper, the reconstruction order is greater than 5. Effective suppression of the side lobes of the correlation function is achieved. The interference bandwidth affects the splitting degree of the navigation signal spectrum, which in turn affects the lifting degree of the side lobes of the correlation function. From the simulation results, when the reconstruction order is 10, the method proposed in this paper can effectively suppress the sidelobes, and the suppression performance is good. The amplitude estimation of the navigation signal is the core of the method in this paper. The accuracy of the amplitude estimation directly determines the performance of the sidelobe suppression. According to the simulation results, the sidelobe suppression performance is closely related to the accuracy of the amplitude estimation. When the magnitude is small, the inhibition effect becomes greater, and the influence is slightly smaller when the magnitude estimate is too large, so the magnitude estimate can be appropriately enlarged in practical applications.

## 7. Conclusions

In this paper, a navigation signal correlation function sidelobe suppression method based on time-domain adaptive anti-jamming processing in satellite navigation receivers

is proposed, which solves the problem of the degradation of acquisition performance caused by the rise of the correlation function sidelobes. The narrow-band interference suppression based on time-domain adaptive anti-jamming will cause the side lobe of the navigation signal to rise, resulting in the degradation of the acquisition performance. This paper analyzes the mechanism of the side lobe lift of the correlation function caused by the time-domain adaptive anti-jamming and proposes a method to suppress the side lobe of the correlation function according to the mechanism. Simulation experiments show that the theoretical analysis mechanism is correct, and the proposed method can effectively solve the sidelobes suppression caused by time-domain anti-jamming. According to the simulation results, when the reconstruction value is greater than 5 and the accuracy of signal amplitude estimation is between 0.8 and 1.6, the sidelobe can be significantly suppressed. The sidelobe suppression method proposed in this paper improves the sidelobe suppression ratio, eases the difficulty of acquisition in navigation signal processing, and can improve the acquisition performance of navigation signals without sacrificing anti-jamming performance.

**Author Contributions:** W.L., Z.L. (Zukun Lu) and J.S. performed the theoretical study, conducted the experiments, processed the data and wrote the manuscript. Z.W. (Zhiying Wang), X.L. and W.X. designed the system, provided research suggestions and revised the manuscript. Z.L. (Zongnan Li), Z.W. (Zhi Wang) and J.Q. helped in performing the experiments. X.Y. and B.L. provided the experiment equipment and suggestions for the manuscript. All authors have read and agreed to the published version of the manuscript.

**Funding:** This research was supported in part by the National Natural Science Foundation of China (NSFC), grants 62003354.

**Acknowledgments:** The authors would like to thank the editors and reviewers for their efforts to help the publication of this paper.

**Conflicts of Interest:** The authors declare that they have no conflict of interest.

## References

1. Ladina, S.; Michael, M.; Christoph, M. Impact of GPS processing on the estimation of snow water equivalent using refracted GPS signals. *IEEE Trans. Geosci. Remote Sens.* **2020**, *58*, 123–135.
2. Camps, A. Spatial Resolution in GNSS-R Under Coherent Scattering. *IEEE Geosci. Remote Sens. Lett.* **2020**, *17*, 32. [[CrossRef](#)]
3. Zhang, P.; Tu, R.; Zhang, R.; Gao, Y.; Cai, H. Combining GPS, BeiDou, and Galileo Satellite Systems for Time and Frequency Transfer Based on Carrier Phase Observations. *Remote Sens.* **2018**, *10*, 324. [[CrossRef](#)]
4. Chen, H.; Niu, F.; Su, X.; Gegn, T.; Liu, Z.; Li, Q. Initial Results of Modeling and Improvement of BDS-2/GPS Broadcast Ephemeris Satellite Orbit Based on BP and PSO-BP Neural Networks. *Remote Sens.* **2021**, *13*, 4801. [[CrossRef](#)]
5. Yi, T.-H.; Li, H.-N.; Gu, M. Experimental assessment of high-rate GPS receivers for deformation monitoring of bridge. *Measurement* **2013**, *46*, 420. [[CrossRef](#)]
6. Chertova, O.G.; Chirov, D.S. Development Prospects of the ERA-GLONASS System. In Proceedings of the 2022 Wave Electronics and Its Application in Information and Telecommunication Systems (WECONF), St-Petersburg, Russia, 30 May 2022. [[CrossRef](#)]
7. Elghamrawy, H.; Karaim, M.; Korenberg, M.; Noureldin, A. High-Resolution Spectral Estimation for Continuous Wave Jamming Mitigation of GNSS Signals in Autonomous Vehicles. *IEEE Trans. Intell. Transp. Syst.* **2022**, *23*, 7881–7895. [[CrossRef](#)]
8. Rezazadeh, N.; Shafai, L. A Compact Antenna for GPS Anti-Jamming in Airborne Applications. *IEEE Access* **2019**, *7*, 154253–154259. [[CrossRef](#)]
9. Liu, Y.; Zhang, S.; Gao, Y. A High-Temperature Stable Antenna Array for the Satellite Navigation System. *IEEE Antennas Wirel. Propag. Lett.* **2017**, *16*, 1397–1400. [[CrossRef](#)]
10. Lu, Z.; Chen, F.; Xie, Y.; Sun, Y.; Cai, H. High Precision Pseudo-Range Measurement in GNSS Anti-jamming Antenna Array Processing. *Electronics* **2020**, *9*, 412. [[CrossRef](#)]
11. Chien, Y.-R. Design of GPS Anti-Jamming Systems Using Adaptive Notch Filters. *IEEE Syst. J.* **2015**, *9*, 451–460. [[CrossRef](#)]
12. Chaparro, D.; Afeldman, F.; Chaubell, M.J.; Yueh, S.H.; Entekhabi, D. Robustness of Vegetation Optical Depth Retrievals Based on L-Band Global Radiometry. *IEEE Trans. Geosci. Remote Sens.* **2022**, *60*, 4413417. [[CrossRef](#)]
13. Xu, W.; Xing, W.; Fang, C.; Huang, P.; Tan, W.; Gao, Z. RFI Suppression for SAR Systems Based on Removed Spectrum Iterative Adaptive Approach. *Remote Sens.* **2020**, *12*, 3520. [[CrossRef](#)]
14. Marathe, T.; Daneshmand, S.; Lachapelle, G. Assessment of Measurement Distortions in GNSS Antenna Array Space-Time Processing. *Int. J. Antennas Propag.* **2016**, *2*, 1–17. [[CrossRef](#)]
15. Lu, Z.; Chen, H.; Chen, F.; Nie, J.; Ou, G. Blind Adaptive Channel Mismatch Equalization Method for GNSS Antenna Arrays. *IET Radar Sonar Navig.* **2018**, *12*, 383–389. [[CrossRef](#)]

16. Zhou, Q.; Zheng, H.; Wu, X.; Yue, X.; Chen, Z.; Wang, Q. Fractional Fourier Transform-Based Radio Frequency Interference Suppression for High-Frequency Surface Wave Radar. *Remote Sens.* **2020**, *12*, 75. [[CrossRef](#)]
17. Gao, G.X.; Sgammini, M.; Lu, M.; Kubo, N. Protecting GNSS Receivers From Jamming and Interference. *Proc. IEEE* **2016**, *104*, 1327–1338. [[CrossRef](#)]
18. Song, J.; Lu, Z.; Xiao, Z.; Li, B.; Sun, G. Optimal Order of Time-Domain Adaptive Filter for Anti-jamming Navigation Receiver. *Remote Sens.* **2022**, *14*, 48. [[CrossRef](#)]
19. Bertold, V.D.B.; Sofie, P. Keeping UAVs under control during GPS jamming. *IEEE Syst. J.* **2019**, *13*, 2010–2021.
20. Lu, Z.; Nie, J.; Chen, F.; Ou, G. Impact on Anti-jamming Performance of Channel Mismatch in GNSS Antenna Arrays Receivers. *Int. J. Antennas Propag.* **2016**, *2016*, 1909708. [[CrossRef](#)]
21. Kim, S.; Park, K.; Seo, J. Mitigation of GPS Chirp Jammer Using a Transversal FIR Filter and LMS Algorithm. In Proceedings of the 34th International Technical Conference on Circuits/Systems, Computers and Communications (ITC-CSCC), Jeju, Korea, 23–26 June 2019. [[CrossRef](#)]
22. Nouri, M.; Aghdam, S.A.; Vakili, V.T. An optimal method for narrowband interference mitigation in the GPS. In Proceedings of the Fourth International Conference on Modeling, Simulation and Applied Optimization, Kuala Lumpur, Malaysia, 19–21 April 2011. [[CrossRef](#)]
23. Cheng, L.; Wang, K.; Ren, M.; Yan, G. Adaptive Filter Approach for GPS Multipath Estimation Under Correntropy Criterion in Dynamic Multipath Environment. *IEEE Trans. Signal Process.* **2019**, *67*, 5798–5810. [[CrossRef](#)]
24. Lu, Z.; Nie, J.; Wan, Y.; Ou, G. Optimal reference element for interference suppression in GNSS antenna arrays under channel mismatch. *IET Radar Sonar Navig.* **2017**, *11*, 1161–1169. [[CrossRef](#)]
25. Compton, R.T. The power-inversion adaptive array: Concept and performance. *IEEE Trans. Aerosp. Electron. Syst.* **1979**, *15*, 803–814. [[CrossRef](#)]
26. Jie, W.; Liu, W.; Chen, F.; Lu, Z.; Gang, O. GNSS array receiver faced with overloaded interferences: Anti-jamming performance and the incident directions of interferences. *J. Syst. Eng. Electron.* **2022**, *99*, 1–7. [[CrossRef](#)]
27. Lu, Z.; Nie, J.; Chen, F.; Chen, H.; Ou, G. Adaptive Time Taps of STAP Under Channel Mismatch for GNSS Antenna Arrays. *IEEE Trans. Instrum. Meas.* **2017**, *66*, 2813–2824. [[CrossRef](#)]
28. Lu, Z.; Song, J.; Huang, L.; Ren, C.; Xiao, Z.; Li, B. Distortionless 1/2 Overlap Windowing in Frequency Domain Anti-Jamming of Satellite Navigation Receivers. *Remote Sens.* **2022**, *14*, 1801. [[CrossRef](#)]
29. Fan, G. Research on High Precision Ranging Technology of Anti-Jamming Receiver under Non-Ideal Channel. Doctoral Dissertation, National University of Defense Technology, Changsha, China, 2016.
30. Zhou, Z.; Wei, Y. The Influence of Automatic Gain Control on Narrowband Frequency Domain GPS Anti-Jamming Receiver. In Proceedings of the IEEE 21st International Conference on Communication Technology (ICCT), Tianjin, China, 13–16 October 2021. [[CrossRef](#)]
31. Li, X.; Chen, F.; Lu, Z.; Liu, Z.; Ou, G. Overview of Anti-Jamming Technology Based on GNSS Single-Antenna Receiver. In Proceedings of the 3rd International Conference on Geoinformatics and Data Analysis (ICGDA), Marseille, France, 15–17 April 2020. [[CrossRef](#)]
32. Zhang, T.; Zhao, H.; Cui, X.; Lu, M. The Upper Bound of Anti-Jamming Capability for GNSS Receivers with Finite Quantization Bits. In Proceedings of the China Satellite Navigation Conference (CSNC), Beijing, China, 22–25 May 2012. [[CrossRef](#)]
33. Blinchikoff, H.J. Range sidelobe reduction for the quadriphase codes. *IEEE Trans. Aerosp. Electron. Syst.* **1996**, *32*, 668–675. [[CrossRef](#)]
34. Li, Z. Research on Anti-Jamming Technology of Satellite Positioning Receiver. Ph.D. Thesis, National University of Defense Technology, Changsha, China, 2004.
35. Xue, B.; Gai, M.; Shen, F.; Liu, N. A novel method of multipath mitigation for C/A code tracking loop based on wavelet transform. In Proceedings of the IEEE International Conference on Information and Automation, Shenzhen, China, 6–8 June 2011. [[CrossRef](#)]
36. Gao, Y.; Xie, S. A variable step size LMS adaptive filtering algorithm and analysis. *Chin. Electron. J.* **2001**, *29*, 1094–1097.
37. Liu, Y.-J.; Hu, H.-Y. The Research on GPS Frequency Domain Anti-Jamming Algorithms. In Proceedings of the 5th International Conference on Wireless Communications, Networking and Mobile Computing, Beijing, China, 24 September 2009. [[CrossRef](#)]
38. Cui, J.; Chen, N.; He, P. Adaptive anti jamming algorithm for GNSS software receiver. In Proceedings of the IEEE Information Technology, Networking, Electronic and Automation Control Conference, Chongqing, China, 20–22 May 2016. [[CrossRef](#)]
39. Savas, C.; Falco, G.; Dosis, F. A Comparative Performance Analysis of GPS L1 C/A, L5 Acquisition and Tracking Stages Under Polar and Equatorial Scintillations. *IEEE Trans. Aerosp. Electron. Systems.* **2021**, *57*, 227–244. [[CrossRef](#)]
40. Schmidt, E.; Gatsis, N.; Akopian, D. A GPS Spoofing Detection and Classification Correlator-Based Technique Using the LASSO. *IEEE Trans. Aerosp. Electron. Syst.* **2020**, *56*, 4224–4237. [[CrossRef](#)]